

A Note on the Relationship between Temperature and Water Vapor
in Quasi-Equilibrium and Climate States

by

C.-L. Shie^{1,2}, W.-K. Tao², J. Simpson² and C.-H. Sui³

¹Goddard Earth Sciences and Technology Center

University of Maryland, Baltimore County

Baltimore, Maryland 21250

²Laboratory for Atmospheres

NASA Goddard Space Flight Center

Greenbelt, Maryland 20771

³Institute of Hydrological Sciences

National Central University/College of Earth Sciences

Jung-Li, Taiwan

J. of Climate

(February 7, 2005)

Corresponding author address: Dr. Chung-Lin Shie, Mesoscale Atmospheric Processes

Branch, Code 613.1, NASA/GSFC, Greenbelt, MD 20771

e-mail: shie@agnes.gsfc.nasa.gov

Abstract

An ideal and simple formulation is successfully derived that well represents a quasi-linear relationship found between the domain-averaged water vapor, q (mm), and temperature, T (K), fields obtained from a series of quasi-equilibrium (long-term) simulations for the Tropics using the two-dimensional Goddard Cumulus Ensemble (GCE) model. Earlier model work showed that the forced maintenance of two different wind profiles in the Tropics leads to two different equilibrium states. Investigating this finding required investigation of the slope of the moisture-temperature relations, which turns out to be linear in the Tropics. The extra-tropical climate equilibriums become more complex, but insight on modeling sensitivity can be obtained by linear stepwise regression of the integrated temperature and humidity. A globally curvilinear moisture-temperature distribution, similar to the famous Clausius-Clapeyron curve (i.e., saturated water vapor pressure versus temperature), is then found in this study. Such a genuine finding clarifies that the dynamics are crucial to the climate (shown in the earlier work) but the thermodynamics adjust. The range of validity of this result is further examined herein. The GCE-modeled tropical domain-averaged q and T fields form a linearly-regressed “ q - T ” slope of 4.218 ($mm K^{-1}$) that genuinely resides within an “ideal” range of slopes (i.e., C_{ideal} between 4.016 and 4.462) obtained from the aforementioned formulation. A quantity (denoted as dC_2/dC_1) representing the derivative between the static energy densities ($J m^{-2}$) due to temperature (C_2) and water vapor (C_1) for various quasi-equilibrium states can also be obtained. A dC_2/dC_1 value near unity obtained for the GCE-modeled tropical simulations implies that the static energy densities due to moisture and temperature only differ by a pure constant for various equilibrium states. An overall q - T relation also including extra-tropical regions is, however, found to have a curvilinear relationship. Accordingly, warm/moist regions (i.e., $dC_2/dC_1 > 1$) favor change in water vapor faster than temperature, while cold/dry regions favor an increase in temperature quicker than water vapor (i.e., $dC_2/dC_1 < 1$).

1. Introduction

In recent years, cloud-resolving models (CRMs) have been used as a sophisticated and flexible numerical tool to study the role of clouds in the energy and hydrological cycles (as well as the numerically-generated quasi-equilibrium thermodynamic states) in the tropical radiative-convective system (e.g., Islam et al. 1993; Held et al. 1993; Randall et al. 1994; Sui et al. 1994; Grabowski et al. 1996; Robe and Emanuel 1996; Tao et al. 1999; Wu and Moncrieff 1999; Xu and Randall 1999; Tao et al. 2001; Shie et al. 2003; and others). Among these studies (see brief summaries in Tao et al. 1999 and Shie et al. 2003), two distinct two-dimensional (2D) CRM simulations produced by Sui et al. (1994) and Grabowski et al. (1996) showed considerably different quasi-equilibrium states. In an attempt to resolve such a significant numerical finding, a series of systematic numerical studies were recently performed (Tao et al. 1999; Tao et al. 2001; and Shie et al. 2003) over a tropical oceanic domain using the 2D Goddard Cumulus Ensemble (GCE) model with imposed initial conditions taken from the 1956 Marshall Islands Experiment (originally used in Sui et al. 1994 and Grabowski et al. 1996). The plausible dynamical and physical causes that accounted for such a significant discrepancy in the modeled quasi-equilibrium state were genuinely identified and elaborated on in these studies. One striking feature that emerged as a result was a quasi-linear relationship between domain-averaged temperature (K) and water vapor (mm). It was identified and briefly noted in Tao et al. (1999) (also see their Fig. 3). However, whether or not there might be a physical or thermodynamic concept that could plausibly explain this quasi-linearity remained unclear.

The purpose of this note is, therefore, to further clarify (1) what this quasi-linear relation in the GCE-simulated tropical temperature and water vapor fields implies, as well as whether a similar quasi-linear relation will also hold for a tropical group also including observations and additional modeled results, and (2) what kind of temperature-water vapor relation/distribution

may occur in the extra-tropics (i.e., in mid- and high-latitudes). In addition to the series of GCE numerical experiments using the Marshall Islands sounding, observations obtained from two of the major TRMM (Tropical Rainfall Measuring Mission -- Simpson et al. 1996) field experiments [i.e., SCSMEX (the 1998 South China Sea Monsoon Experiment -- Lau et al. 2000) and KWAJEX (the 1999 Kwajalein Atoll field experiment -- Yuter et al. 2004)] as well as from two other field experiments [i.e., TOGA-COARE (Tropical Ocean and Global Atmosphere Coupled Ocean-Atmosphere Response Experiment -- Webster and Lukas 1992) and GATE (Global Atmospheric Research Programme Atlantic Experiment -- Houze and Betts 1981)] are included in this study. GEOS-3 [Goddard EOS (Earth Observing System) Version-3] global re-analysis products (Hou et al. 2001) are also selectively examined and not just for tropical regions but particularly for extra-tropical regions.

The GCE numerical experiments as well as observations from the field experiments, and the GEOS-3 re-analysis data are described in section 2. Section 3 presents a detailed derivation of the idealized theoretical relations representing the slopes of the domain-averaged water vapor and temperature distributions. These theoretical relations are ideally obtained based on a thermodynamic concept. Section 4 presents the major findings and discusses the relationship between the water vapor and temperature distributions (i.e., via the “slope” representation of water vapor versus temperature) based on the numerically simulated results and sounding observations for the Tropics, various latitudinal bands, and the globe, respectively. A final remark is given in section 5.

2. Model-simulated and observed data

a. GCE simulations

There are sixteen (or eight pairs) idealized, tropical simulations from the GCE model (integrated for twenty-five days so as to reach or near statistically quasi-equilibrium states) chosen for presentation in this note. Six (three pairs) of these sixteen runs are the same as those in Shie et al. (2003) that involve various model setups pertaining to two major components: the vertical wind shear pattern and the minimum surface wind speed used for surface flux computation (see details in Table 1a and Fig. 1 of Shie et al. 2003). These three pairs all use the same sounding setup following Sui et al. (1994). One other pair of runs have a similar model setup to one of the three mentioned pairs except for using the sounding setup from Grabowski et al. (1996). Each of the remaining four pairs of runs have an overall similar model setup to the “control” runs in Shie et al. (2003, i.e., the second pair in their Table 1a) except for one distinct component of the large-scale conditions such as large-scale forcing, surface fluxes, radiation, and sea surface temperature, respectively.

b. Observed data and GEOS-3 re-analysis

In addition to the single sounding from the Marshall Islands that was used in the GCE simulations, eight time series of tropical temperature and water vapor observations are also applied in this study mainly to populate the sample tropical observations for analysis. They include two episodes from SCSMEX (one from the summer monsoon onset period during May 18-26, 1998, and one from the post-onset period during June 2-11, 1998), three episodes from KWAJEX (Aug 7-12, Aug 17-21, and Aug 29-Sep 13, 1999), two episodes from TOGA-COARE (Dec 10-17, and Dec 19-27, 1992), and one episode from GATE (Dec 1-8, 1974). The readily accessible GEOS-3 re-analysis data are also included here to increase the sample data points in the Tropics, as well as to extend the sample data points to extra-tropical regions. The GEOS-3 re-analysis data selected are the monthly-averaged products that include (1) seven “summer” months – May, June, July and August in 1998 for SCSMEX and July, August and September in 1999 for KWAJEX, and (2) four “winter” months – January, February,

November, and December in 1998. The GEOS-3 "summer" months were intended to match the SCSMEX and KWAJEX periods, while the "winter" months were chosen for the same year as SCSMEX - 1998. Details of how these eleven selected GEOS-3 monthly data have been examined will be addressed later along with the respective discussions.

3. Relations between temperature and water vapor

Horizontal integration (average) of the equations for potential temperature (θ), and water vapor (mixing ratio, q_v) over the model domain yields

$$C_p \frac{\partial \bar{T}}{\partial t} = (L_v(\bar{c} - \bar{e}) + L_s(\bar{d} - \bar{s}) + L_f(\bar{f} - \bar{m})) - C_p \bar{\pi} \bar{w} \frac{\partial \bar{\theta}}{\partial z} - C_p \bar{\pi} \frac{1}{\bar{\rho}} \frac{\partial}{\partial z} \bar{\rho} \bar{w}' \theta' + \bar{Q}_R, \quad (1)$$

and

$$L_v \frac{\partial \bar{q}_v}{\partial t} = -(L_v(\bar{c} - \bar{e}) + L_s(\bar{d} - \bar{s})) - L_v \bar{w} \frac{\partial \bar{q}_v}{\partial z} - L_v \frac{1}{\bar{\rho}} \frac{\partial}{\partial z} \bar{\rho} \bar{w}' q_v' \quad (2)$$

where variables with an overbar are horizontal-averaged quantities, and deviations from the means are denoted by a prime, while c , e , d , s , f and m are condensation, evaporation, deposition, sublimation, freezing, and melting, respectively. T is temperature, and $\bar{\pi} = (p/P_{00})^{R/C_p}$ is the nondimensional pressure, where p is the dimensional pressure and P_{00} the reference pressure taken to be 1000 mb. C_p is the specific heat of dry air at constant pressure, and R is the gas constant for dry air. $-\bar{w} \frac{\partial \bar{\theta}}{\partial z}$ and $-\bar{w} \frac{\partial \bar{q}_v}{\partial z}$ are the mean advection of potential temperature (cooling) and water vapor (moistening); \bar{w} is the prescribed large-scale mean vertical velocity

(constant with time); $\frac{\partial \bar{\theta}}{\partial z}$ and $\frac{\partial \bar{q}_v}{\partial z}$ are model mean vertical potential temperature and water vapor gradients (varying with time); $-\frac{1}{\bar{\rho}} \frac{\partial}{\partial z} \overline{\rho w' \theta'}$ and $-\frac{1}{\bar{\rho}} \frac{\partial}{\partial z} \overline{\rho w' q'_v}$ are the vertical eddy flux convergence/divergence for potential temperature and water vapor, respectively. Q_R is the radiative heating containing solar and infrared radiation. The variables L_v , L_f , and L_s are the latent heats of condensation, fusion and sublimation, respectively. For an equilibrium state, the vertically integrated equations (1) and (2) can be reduced to

$$C_p \frac{\partial \{\bar{T}\}}{\partial t} = 0, \quad (3)$$

and

$$L_v \frac{\partial \{\bar{q}_v\}}{\partial t} = 0 \quad (4)$$

where $\{\bar{T}\}$ and $\{\bar{q}_v\}$ are the domain-averaged and density-weighted temperature (K), and the vertically integrated column water vapor (mm) (so called "precipitable water"), respectively. The units for $\{\bar{q}_v\}$ are in mm since \bar{q}_v ($g\ kg^{-1}$) has been integrated along a vertical column with the vertical scale height becoming implicit. Curly parentheses are thus used to denote such a vertical integral for water vapor to distinguish from the brackets that represent a vertical average for temperature (along with an explicit vertical scale height). The vertically-integrated static energy densities ($J\ m^{-2}$) from the domain-averaged temperature and water vapor, respectively, at an equilibrium state (i.e., $C_1(\tau)$ and $C_2(\tau)$ with τ representing various equilibrium states) can then be represented as follows:

$$C_1(\tau) = C_p \bar{\rho}_{air} [\bar{T}] H, \quad (5)$$

$$C_2(\tau) = L_v \bar{\rho}_w \{\bar{q}_v\} \quad (6)$$

where $\bar{\rho}_{air}$ and $\bar{\rho}_w$ are the domain-averaged air and water vapor densities and H the vertical scale height of the free atmosphere. By taking the derivative of equation (6) over equation (5) and assuming that $\bar{\rho}_{air}$ and $\bar{\rho}_w$ are invariant for various quasi-equilibrium states and that the derivative change of L_v with temperature is negligible, a theoretical relationship between the variations of water vapor and temperature with respect to quasi-equilibrium state can then be obtained as follows

$$\frac{d\{\bar{q}_v\}}{d[\bar{T}]} = (C_p \bar{\rho}_{air} H / L_v \bar{\rho}_w) \frac{dC_2(\tau)}{dC_1} \quad (7)$$

By assuming that $\bar{\rho}_w$ is 10^3 times that of $\bar{\rho}_{air}$ (e.g., 10^3 versus 1 kg m^{-3}) and H is 10 km , equation (7) can be further simplified as

$$\frac{d\{\bar{q}_v\}}{d[\bar{T}]} = C_{ideal} \frac{dC_2(\tau)}{dC_1} \quad (8)$$

where $C_{ideal} = (C_p / L_v)(10^4 \text{ mm})$ and increases from $4.016 \text{ (mm K}^{-1}\text{)}$ to $4.462 \text{ (mm K}^{-1}\text{)}$ as L_v decreases from $2.5 \times 10^6 \text{ J kg}^{-1}$ (at 0°C) to $2.25 \times 10^6 \text{ J kg}^{-1}$ (at 100°C) at a C_p of $1004 \text{ J (K kg)}^{-1}$. Equation (8) provides a simplified theoretical relationship for the “derivative/distribution of $\{\bar{q}_v\}$ and $[\bar{T}]$ ” (denoted as “ $\{(\bar{q}_v), [\bar{T}]\}$ ” hereafter) that depends on a near constant C_{ideal} (e.g.,

between $0^{\circ}C$ and $100^{\circ}C$) and dC_2/dC_1 . Under a special condition when the static energy contribution from temperature (C_1) and moisture (C_2) only differ by a pure constant for various equilibrium states τ (i.e., dC_2/dC_1 equals one), the slope of $(\{\bar{q}_v\}, [\bar{T}])$ in equation (8) can then be reduced to C_{ideal} . Note that C_{ideal} increases with increasing temperature (i.e., decreasing L_v), although such variations can be negligible.

4. Results

Similar to the three previous studies (i.e., Tao et al. 1999, Tao et al. 2001, and Shie et al. 2003) mentioned in the introduction, the current sixteen GCE-simulated experiments presented here (denoted as “GCE-T” and shown as dark circles in Fig. 1) also show a quasi-linear relationship between $\{\bar{q}_v\}$ and $[\bar{T}]$ at their quasi-equilibrium states (after 25 days of integration). A linear regression method built into the plotting package (“KaleidaGraph”) that produced the scatter plot has also been applied to the data group shown in Fig. 1 to obtain the regression line as well as the value of its slope. Based on Eq. 8, an approximate value of dC_2/dC_1 is also obtained by dividing the associated slope value by an average value for C_{ideal} [i.e., $4.239 (mm K^{-1})$, the mean of $4.016 (mm K^{-1})$ and $4.462 (mm K^{-1})$]. Accordingly, the GCE tropical simulations (GCE-T) are found to have a slope of 4.218, which is within the “ideal range of C_{ideal} ” (i.e., from 4.016 to 4.462), as well as a dC_2/dC_1 value of 0.995, which is near unity where C_1 and C_2 only differ by a pure constant for various equilibrium states. The value of dC_2/dC_1 for the GCE-T data is also listed in Table 1, along with those from groups addressed in later discussions.

In addition to the sixteen GCE tropical simulations, forty-two more tropical data points consisting of nine sounding observations and thirty-three GEOS-3 “tropical” simulations

(including twenty-one "summer" and twelve "winter" months) are also included in the tropical regime (denoted as "Tropics" hereafter). There are three tropical regions (approximating the sites of SCSMEX, KWAJEX, and TOGA-COARE) from GEOS-3 separated into seven "summer" and four "winter" months; therefore, there are twenty-one and twelve data points for "summer" and "winter" months, respectively. In order to investigate the water vapor-temperature relationship in extra-tropical regions and the entire global domain, the GEOS-3 data for the seven "summer" and four "winter" months were sorted into six latitudinal bands for two "seasons" and were also globally averaged. Similar to GCE-T, the dC_2/dC_1 values representing the moisture-temperature distributions for the three aforementioned groups, the "Tropics" (fifty-eight points), the twelve "seasonal" latitudinal regions, and the global averages (denoted as "Global", the eleven monthly-averaged data) are computed and listed either in the relatively "warm/moist" or "cold/dry" region in Table 1 corresponding to their thermodynamic states. Two extra groups "Lat-WM" and "Lat-CD" consisting of the respective six cases of relatively warm/moist and cold/dry latitudinal bands are also included in Table 1. The associated moisture-temperature distributions for the "Tropics" (dark circles along a thick dashed line), Lat-WM (crosses along a thick solid line), Lat-CD (open circles along a thick dotted line), and "Global" (open triangles along a solid line) are shown in Fig. 2.

Fig. 2 and Table 1 show that the slope of $(\{\bar{q}_v\}, \bar{T})$ and the value of dC_2/dC_1 generally increase with temperature (or the thermodynamic equilibrium state). The "Tropics" (thick dashed line in Fig. 2) have a large dC_2/dC_1 value (i.e., 1.318), which is larger than the 0.995 value of GCE-T (thick dashed line in Fig. 1), and those (ranging from 0.035 for "SH-sum" to 1.137 for "SL-win") of all the "seasonal" latitudinal bands. A group of tropical observations included in the "Tropics" has a dC_2/dC_1 value of 1.606 (not shown in Table 1) that accounts for the larger dC_2/dC_1 of the "Tropics". As for the latitudinal bands, most of the warm/moist

regions (i.e., SL-win, NL-sum, and SL-sum if NL-win is not included) possess values of dC_2/dC_1 near or greater than one (i.e., slope values within or larger than the ideal range of C_{ideal}), while all of the cold/dry regions have values of dC_2/dC_1 much less than one (i.e., very small slopes). The only group with a negative slope value (NL-win with four points) might have had a much larger positive slope if more data points were available. Unsurprisingly, "Global" (consisting of seven "summer" and four "winter" months) has a dC_2/dC_1 value of 0.405 that is lower than most of the warm/moist region and higher than the cold/dry regions. "Global" is listed in the cold/dry region in Table 1 simply to be in contrast to the "Tropics". However, the group of four global "winter" months alone has a much smaller dC_2/dC_1 value (i.e., 0.178) than that (i.e., 0.408) of the seven global "summer" months (not shown in Table 1). In Fig. 2, Lat-WM (thick solid line) and Lat-CD (thick dotted line), which include the respective six cases of relatively warm/moist and cold/dry latitudinal bands¹, support the common finding that the dC_2/dC_1 value is larger and smaller for the summarized warm/moist and cold/dry regimes, respectively. Such a "stepwise-linear" (curvilinear) moisture-temperature distribution (e.g., from a small dC_2/dC_1 for the cold/dry Lat-CD, through a moderate dC_2/dC_1 for the mild Lat-WM, to a large dC_2/dC_1 for the very warm/moist "Tropics") implies that the warm and moist tropical regions tend to favor changes in water vapor faster than temperature ($dC_2/dC_1 > 1$) while the cold and dry high latitudes favor an increase in temperature quicker than water vapor ($dC_2/dC_1 < 1$). This feature of a slower/quicker change in water vapor for a colder/warmer state led to the following investigation. The relative humidity field (RH) obtained from the associated GEOS-3 data has also been examined. Relative humidity is found to change with temperature in an interesting two-branch pattern (shown in Fig. 3). In one branch (covering the mid- and high latitudes),

¹ The linearly regressed lines for each of the twelve latitude bands are not shown in Fig. 2 for the sake of clarity; however, the associated dC_2/dC_1 values are computed and listed in Table 1.

relative humidity roughly decreases from 61-66% around 220-225K to 43-50% around 250-255K due to a slower increase of moisture than saturated moisture with increased temperature, while in the other branch (covering the tropics) relative humidity increases more rapidly from 34-40% around 255K to 60-65% around 260K due to a faster increase of moisture than saturated moisture with increased temperature. However, the high relative humidity shown for the high latitude regions (with low temperature and water vapor) might be overestimated that is suspected to be due to an underestimated saturated humidity at a very low temperature.

All of the moisture-temperature data (135 data points in total) presented in Fig. 2 are also approximated with an exponential fitting (by also using a built-in utility in "KaleidaGraph"), as well as re-plotted in Fig. 4. Fig. 4 genuinely shows a remarkable resemblance between the curvilinear (\bar{q}, \bar{T}) relation (i.e., dark circles and the thick solid line on the left hand side) and the curvilinear relationship between saturated water vapor pressure and temperature obtained from the Clausius-Clapeyron equation (open circles and the exponentially approximated thick dashed line on the right hand side). This similarity seemingly indicates that a fundamental thermodynamic theory may apply over a variety of scales ranging from the micro- to the macro-scale. Previous modeling work (Tao et al. 1999 and Shie et a. 2003) showed that the forced maintenance of two different wind profiles in the Tropics leads to two different equilibrium (three to four weeks) states. These states follow a locally quasi-linear temperature-moisture relation yet are embedded in a globally curvilinear distribution in this paper. Such a genuine moisture-temperature relation clarifies that the dynamics are crucial to the climate (findings in previous works) but the thermodynamic adjusts.

5. Concluding remarks

For the quasi-equilibrium moisture and temperature fields, a theoretical relationship for $(\{\bar{q}_v\}, \bar{T})$ (the derivative/distribution of $\{\bar{q}_v\}$ and \bar{T}) can be constructed (Eq. 8) based on a few simplifications. The obtained ideal slope C_{ideal} that depends on (C_p/L_v) ranges from 4.016 ($mm K^{-1}$) to 4.462 ($mm K^{-1}$) as L_v decreases from $2.5 \times 10^6 J kg^{-1}$ (at $0^\circ C$) to $2.25 \times 10^6 J kg^{-1}$ (at $100^\circ C$) at a C_p of $1004 J (K kg)^{-1}$. On one hand, GCE-T is the only group in this paper where the water vapor and temperature fields were obtained at the modeled quasi-equilibrium states, while those from observations or GEOS-3 simulations were either averages over certain periods (except for the Marshall Islands single sounding) or monthly averages, respectively. On the other hand, GCE-T is also the only group whose slope value of $(\{\bar{q}_v\}, \bar{T})$ falls within the ideal range of C_{ideal} (i.e., dC_2/dC_1 almost equaling unity). These concurrent features might imply that the static energy densities of water vapor and temperature only differ by a pure constant for various tropical equilibrium (or quasi-) states. This feature was approximately shown in the respective static energy of $C_p T$ and $L_v q_v$ presented by Shie et al. (2003) in their Table 7. The “perfect” slope found in GCE-T may be attributed to a robust evolution between the GCE-generated tropical temperature and water vapor fields corresponding to the radiative-convective interaction that are numerically well represented by the explicit cloud-scale dynamics, sophisticated microphysical processes, and explicit cloud-radiation interaction. Basically, latent heating (due to condensation, evaporation, deposition, sublimation, freezing, and melting)/precipitation have played a decisive role in counteracting the imbalance produced between a cycle of radiative destabilization (in general, radiation generated a cooling effect for the air aloft) succeeded by convective stabilization (convection, on the other hand, tended to dry the boundary layer as well as warm the air aloft) in the so-called “radiative-convective oscillations” mechanism that was prevalent in the radiative-convective systems (see details in Randall et al. 1994).

This domain-averaged water vapor and temperature distribution was further extended to extra-tropical regions (i.e., mid- and high latitudes) and the entire globe for both “summer” and “winter” months primarily through the use of GEOS-3 reanalysis data. In general, most of the warm/moist regions tend to favor changes in water vapor faster than temperature ($dC_2/dC_1 > 1$, i.e., a slope value larger than the ideal range of C_{ideal}), while the cold/dry regions favor an increase in temperature quicker than water vapor ($dC_2/dC_1 < 1$, i.e., a slope value smaller than the ideal range of C_{ideal}). Namely, the slope of $(\{\bar{q}_v\}, \bar{T})$ is larger and smaller for the summarized warm/moist and cold/dry regimes, respectively. Moreover, a remarkable resemblance is found between the curvilinear $(\{\bar{q}_v\}, \bar{T})$ relation and the curvilinear relation of saturated water vapor pressure-temperature obtained based on the Clausius-Clapeyron equation. This feature seems to imply that various systems ranging from micro- to macro-scale might be ruled by a simple yet crucial fundamental thermodynamic theory. Earlier studies (Tao et al. 1999 and Shie et al. 2003) showed that dynamics are crucial to determining the climate regime, while the curvilinear moisture-temperature relation presented here suggests that an adjusting role may be equally importantly played by the thermodynamics.

6. Acknowledgments

The authors wish to thank Dr. A. Hou and Ms. S. Zhang for kindly providing us their GEOS-3 global reanalysis temperature and water vapor fields. Special thanks also go to Mr. S. Lang for reading the manuscript with useful comments and Dr. R.-F. Lin for useful discussions. This study is supported by the NASA Headquarters Physical Climate Program and by the NASA TRMM project. The authors are also grateful to Dr. R. Kakar (NASA/HQ) for his support of this research. Acknowledgment is also made to NASA Goddard Space Flight Center for computer time used in the research.

7. References

- Grabowski, W. W., M. W. Moncrieff, and J. T. Kiehl, 1996: Long-term behavior of precipitating tropical cloud systems: A numerical study. *Quart. J. Roy. Meteor. Soc.*, **122**, 1019-1042.
- Held, I. M., R. S. Hemler, and V. Ramaswamy, 1993: Radiative-convective equilibrium with explicit two-dimensional moist convection. *J. Atmos. Sci.*, **50**, 3909-3927.
- Hou, A. Y., S. Zhang, A. da Silva, W. Olson, C. Kummerow, and J. Simpson, 2001: Improving global analysis and short-range forecast using rainfall and moisture observations derived from TRMM and SSM/I passive microwave sensors. *Bull. Amer. Meteor. Soc.*, **81**, 659-679.
- Houze, R. A., Jr., and Betts, A. K., 1981: Convection in GATE. *Rev. Geophys. Space Phys.*, **19**, 541-576.
- Islam, S., R. L. Bras, and K. A. Emanuel, 1993: Predictability of mesoscale rainfall in the Tropics. *J. Appl. Meteor.*, **32**, 297-310.
- Lau, K. M., Y. Ding, J.-T. Wang, R. Johnson, T. Keenan, R. Cifelli, J. Geriach, O. Thiele, T. Rickenbach, S.-C. Tsay, and P.-H. Lin, 2000: A report of the field operations and early results of the South China Sea Monsoon experiment (SCSMEX). *Bull. Amer. Meteor. Soc.*, **81**, 1261-1270.
- Randall, D. A., Q. Hu, K.-M. Xu, and S. K. Krueger, 1994: Radiative-convective disequilibrium. *Atmos. Res.*, **31**, 315-327.

Robe, F. R., and K. A. Emanuel, 1996: Dependence of tropical convection on radiative forcing. *J. Atmos. Sci.*, **53**, 3265-3275.

Shie, C.-L. , W.-K. Tao, J. Simpson and C.-H. Sui, 2003: Quasi-equilibrium states in the tropics simulated by a cloud-resolving model. Part 1: Specific features and budget analyses. *J. Climate*, **16**, 817-833.

Simpson, J., C. Kummerow, W.-K. Tao and R. Adler, 1996: On the Tropical Rainfall Measuring Mission (TRMM). *Meteor. and Atmos. Phys.*, **60**, 19-36.

Sui, C.-H., K. M. Lau, W.-K. Tao, and J. Simpson, 1994: The tropical water and energy cycles in a cumulus ensemble model. Part I: Equilibrium climate. *J. Atmos. Sci.*, **51**, 711-728.

Tao, W.-K., J. Simpson, C.-H. Sui, C.-L. Shie, B. Zhou, K. M. Lau, and M. Moncrieff, 1999: On equilibrium (climate) states simulated by cloud-resolving models. *J. Atmos. Sci.*, **56**, 3128-3139.

_____, C.-L. Shie, and J. Simpson, 2001: Comments on "A sensitivity study of radiative-convective equilibrium in the tropics with a convection-resolving model". *J. Atmos. Sci.*, **58**, 1328-1333.

Webster, P. J., and R. Lukas, 1992: TOGA COARE: The Coupled Ocean-Atmosphere Response Experiment. *Bull. Amer. Meteor. Soc.*, **73**, 1377-1416.

Wu, X. and M. W. Moncrieff, 1999: Effects of sea surface temperature and large-scale dynamics on the thermodynamic equilibrium state and convection over the tropical western Pacific. *J. Geophys. Res.*, **104**, 6093-6100.

Xu, K.-M., and D. A. Randall, 1999: A sensitivity study of radiative-convective equilibrium in the tropics with a convection-resolving model. *J. Atmos. Sci.*, **56**, 3385-3399.

Yuter, S., R. A. Houze Jr., E. A. Smith, T. T. Wilheit, E. Zipser, 2004: Physical characterization of tropical oceanic convection observed in KWAJEX. *J. Appl. Meteor.* (submitted)

Table 1. Values of dC_2/dC_1 for the following groups: (1) sixteen tropical GCE simulations (“GCE-T”), (2) fifty-eight cases from tropical regions (“Tropics”) including GCE-T, nine tropical sounding observations, and thirty-three GEOS-3 tropical cases, (3) sixty-six GEOS-3 “warm/moist” and “cold/dry” cases from six latitudinal bands in seven “summer” months (“sum”: May, June, July, August, and September) and four “winter” months (“win”: January, February, November, and December) in 1998 or 1999, and (4) global averages (“Global”) from the eleven months of GEOS-3 data used in (3). In (3), the two-capital-letter naming convention identifies the two main latitudinal parameters: (a) northern or southern hemisphere, and (b) high (60-90 degrees), middle (30-60), or low latitudes (0-30). For example, “NL” denotes northern hemisphere (“N”) low-latitudes (“L”). “Lat-WM” and “Lat-CD” include the respective six latitudinal bands of relatively warm/moist and cold/dry regions. Values of dC_2/dC_1 are obtained based on Eq. 8 and the use of an averaged value for C_{ideal} [i.e., 4.239 ($mm K^{-1}$), a mean of 4.016 ($mm K^{-1}$) and 4.462 ($mm K^{-1}$)].

	dC_2/dC_1		dC_2/dC_1
	0.995/1.318		0.405
	1.029		0.035
	1.137		0.104
	-0.201		0.047
	0.986		0.208
	0.414		0.257
	0.322		0.234
	0.701		0.110

Figure captions:

Fig. 1. Scatter diagram of domain-averaged water vapor versus temperature for sixteen tropical GCE simulations "GCE-T" (dark circles), along with the results of Sui et al. (1994) denoted by the "S" and Grabowski et al. (1996) denoted by the "G". A regression line (thick dashed line) obtained by applying a linear regression method to the GCE-T data is also shown.

Fig. 2. Scatter diagram of domain-averaged water vapor versus temperature for the following groups: (1) fifty-eight cases in the tropical regions "Tropics" (dark circles) that include GCE-T (shown in Fig. 1), nine tropical sounding observations, and thirty-three GEOS-3 tropical cases, (2) & (3) sixty-six GEOS-3 "warm/moist" and "cold/dry" cases from six latitudinal bands (see details in Table 1). "Lat-WM" (crosses) and "Lat-CD" (open circles) include the respective six latitudinal bands of relatively warm/moist and cold/dry regions, and (4) global averages "Global" (triangles) from the eleven months of GEOS-3 data used in (2) & (3). Similar to Fig. 1, regression lines are obtained for each of the groups presented, i.e., the "Tropics" (thick dashed line), Lat-WM (thick solid line), Lat-CD (thick dotted line), and "Global" (solid line).

Fig. 3. The distribution of domain-averaged relative humidity (%) versus temperature (K) for the tropical and six latitudinal bands using the GEOS-3 data. The curvilinear line is obtained using a second-order power series fitting.

Fig. 4. The curvilinear distribution of domain-averaged water vapor (in mm) versus temperature for 135 data points (dark circles and solid curve; also shown in Fig. 2) and the curvilinear distribution of saturated water vapor pressure (in mb) versus temperature

obtained based on the Clausius-Clapeyron equation (open circles and dashed curve).

The curvilinear lines are obtained using an exponential fitting.

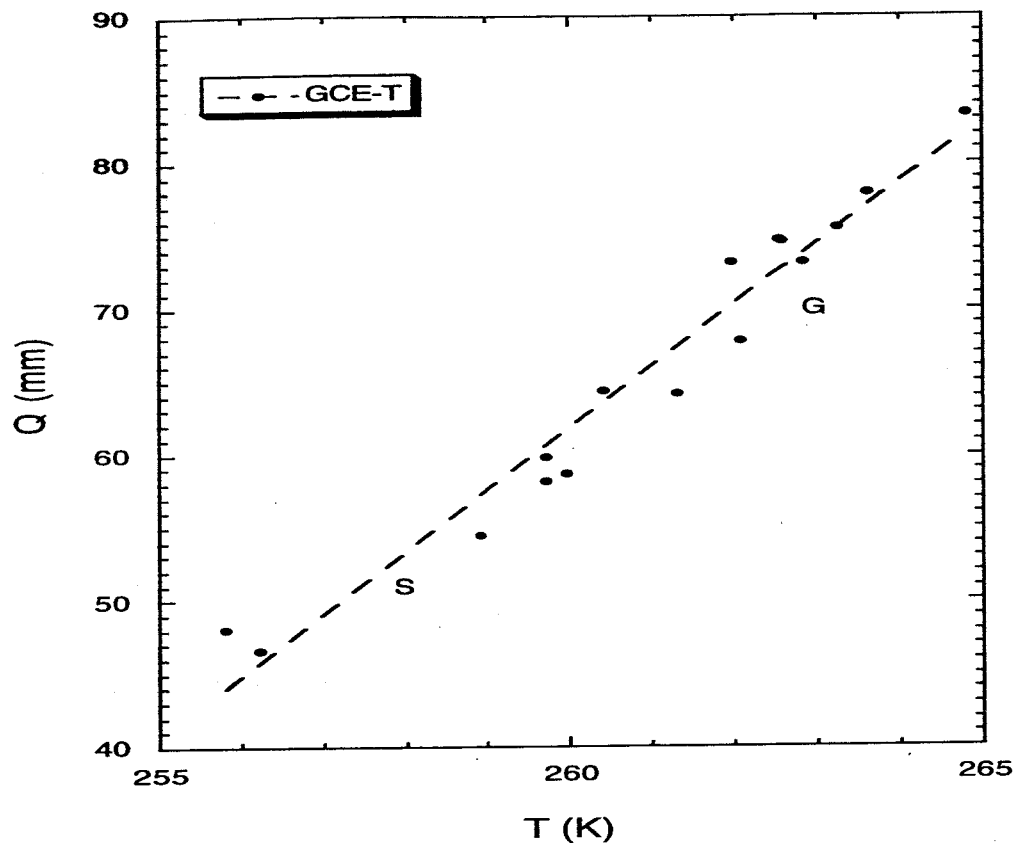


Fig. 1. Scatter diagram of domain-averaged water vapor versus temperature for sixteen tropical GCE simulations "GCE-T" (dark circles), along with the results of Sui et al. (1994) denoted by the "S" and Grabowski et al. (1996) denoted by the "G". A regression line (thick dashed line) obtained by applying a linear regression method to the GCE-T data is also shown.

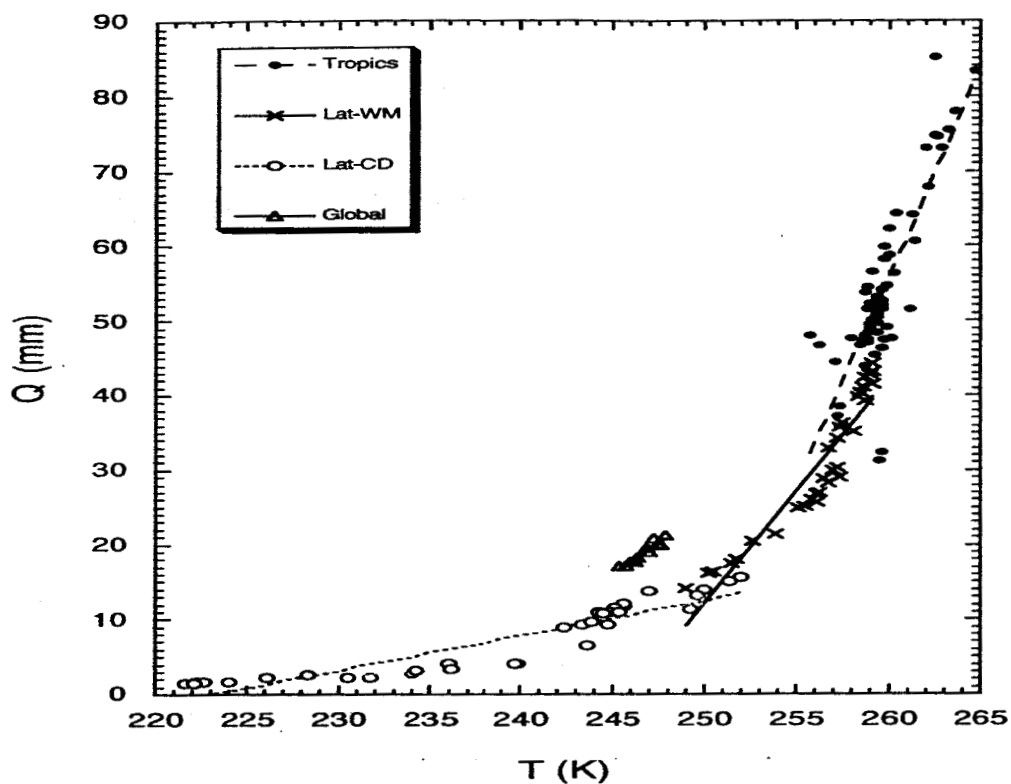


Fig. 2. Scatter diagram of domain-averaged water vapor versus temperature for the following groups: (1) fifty-eight cases in the tropical regions “Tropics” (dark circles) that include GCE-T (shown in Fig. 1), nine tropical sounding observations, and thirty-three GEOS-3 tropical cases, (2) & (3) sixty-six GEOS-3 “warm/moist” and “cold/dry” cases from six latitudinal bands (see details in Table 1). “Lat-WM” (crosses) and “Lat-CD” (open circles) include the respective six latitudinal bands of relatively warm/moist and cold/dry regions, and (4) global averages “Global” (triangles) from the eleven months of GEOS-3 data used in (2) & (3). Similar to Fig. 1, regression lines are obtained for each of the groups presented, i.e., the “Tropics” (thick dashed line), Lat-WM (thick solid line), Lat-CD (thick dotted line), and “Global” (solid line).

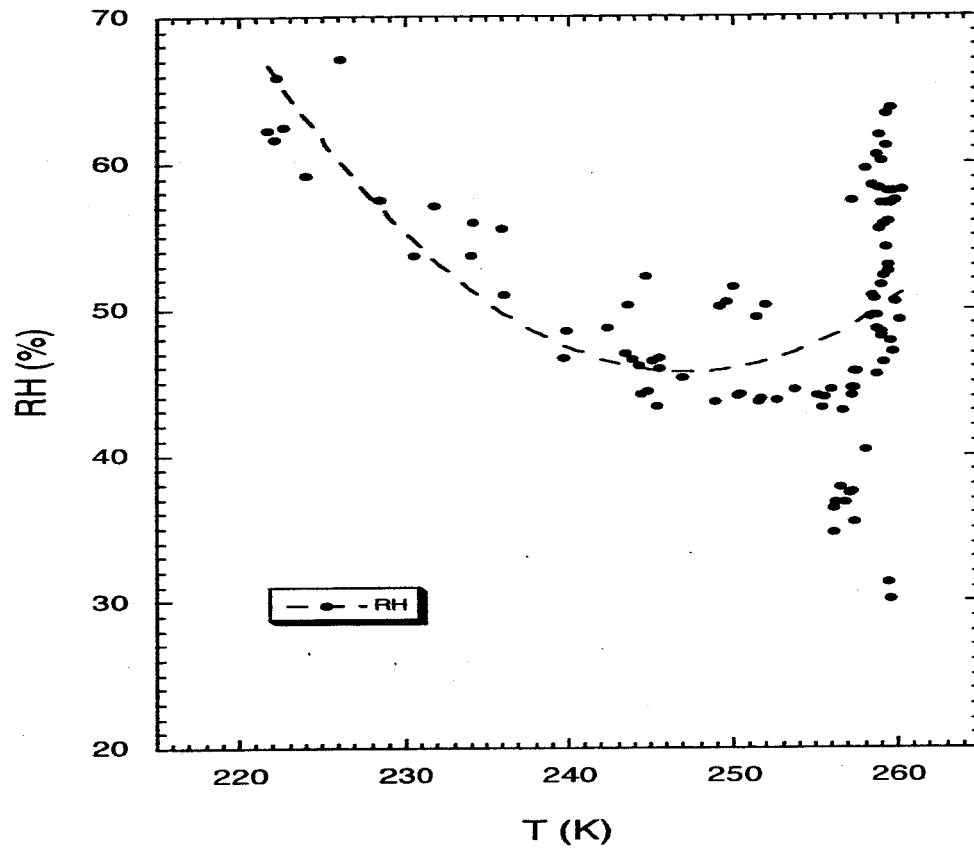


Fig. 3. The distribution of domain-averaged relative humidity (%) versus temperature (K) for the tropical and six latitudinal bands using the GEOS-3 data. The curvilinear line is obtained using a second-order power series fitting.

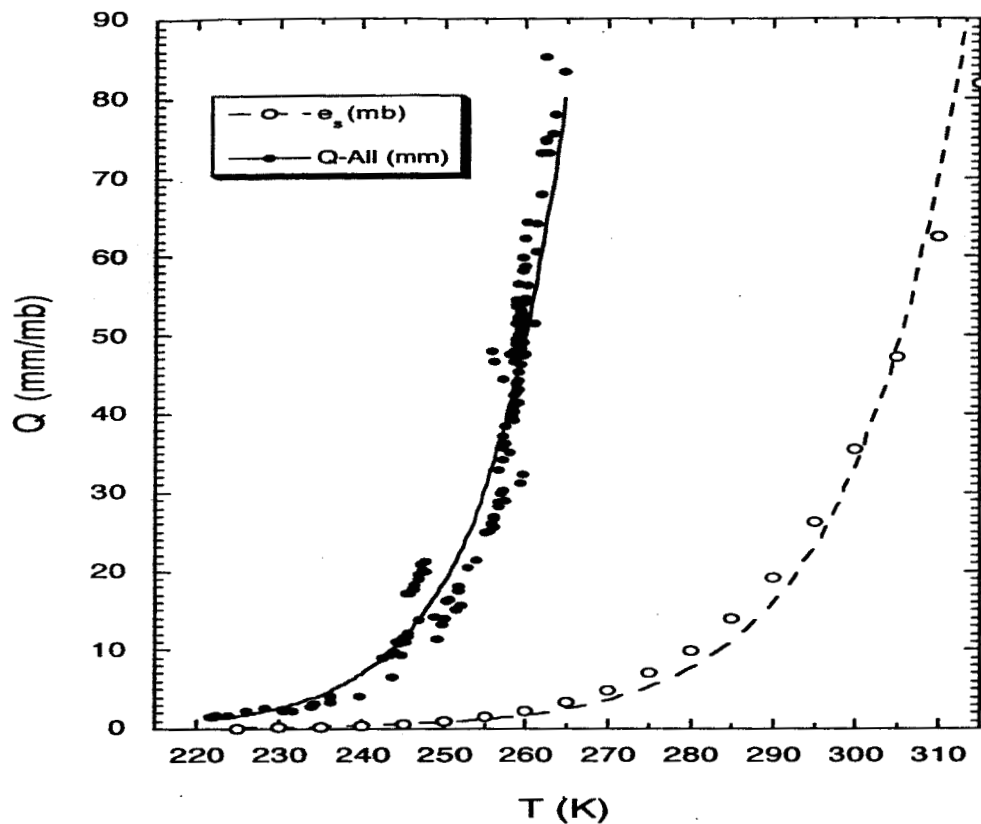


Fig. 4. The curvilinear distribution of domain-averaged water vapor (in mm) versus temperature for 135 data points (dark circles and solid curve; also shown in Fig. 2) and the curvilinear distribution of saturated water vapor pressure (in mb) versus temperature obtained based on the Clausius-Clapeyron equation (open circles and dashed curve). The curvilinear lines are obtained using an exponential fitting.

A Note on the Relationship between Temperature and Water Vapor
in Quasi-Equilibrium and Climate States

C.-L. Shie, W.-K. Tao, J. Simpson, and C.-H. Sui

Popular Summary

An ideal and simple formulation is successfully derived that well represents a quasi-linear relationship found between the domain-averaged water vapor, q (mm), and temperature, T (K), fields obtained from a series of long-term simulations (which reach balanced states) for the Tropics using the two-dimensional Goddard Cumulus Ensemble (GCE) model. Earlier model work showed that two different vertical distributions of horizontal winds in the Tropics lead to two different balanced states. It is further found for the extra-tropical regions that the moisture and temperature have a more complicated relation. The moisture increases with increasing temperature in a curvilinear way, i.e., the moisture increases slower/less at a lower temperature than at a higher temperature. Accordingly, the moisture varies faster/more in the Tropics where weather is relatively warmer and more humid than in high-latitudes where weather is relatively colder and drier. This curvilinear moisture-temperature distribution is very similar to the famous Clausius-Clapeyron curve, i.e., saturated water vapor pressure increases exponentially with increasing temperature. Such a genuine finding clarifies that the dynamics (e.g., the wind fields) are crucial to determine the climate, while the thermodynamics (e.g., the moisture and temperature fields) also play an important role adjusting for a balance between moisture and temperature.